

Transport theory with self-consistent confinement related to the lattice data

P. Bożek*, Y.B. He and J. Hüfner

Institute of Theoretical Physics, Heidelberg University, Philosophenweg 19, D-69120 Heidelberg, Germany
(September 29, 2018)

The space-time development of a quark-gluon plasma is calculated from a Vlasov equation for the distribution function of quasiparticles with medium dependent masses. At each space-time point the masses are calculated selfconsistently from a gap equation, whose form is determined by the requirement that in thermal equilibrium and for a range of temperatures the energy density of the quasi-particle system is identical to the one from lattice calculations. The numerical solutions of the Vlasov equation display confinement. Relations to effective theories like that by Friedberg Lee and Nambu Jona-Lasinio are established.

PACS numbers: 25.75.-q, 12.38.Mh, 12.39.Ba

I. INTRODUCTION

In view of the possible creation of a quark-gluon plasma (QGP) in high-energy heavy ion reactions at the SPS, RHIC and LHC accelerators, descriptions of the space-time evolution of the deconfined phase and its transition into the hadronic phase are very much called for. Ideally, the transport equations should be directly derived from the QCD-Lagrangian, a goal which is not yet achieved. Instead a number of approximate formulations have been proposed. They are either derived from effective Lagrangians (like those by Friedberg Lee [1] or Nambu Jona-Lasinio [2] (NJL)) or they are of Monte-Carlo cascade type [3] with experimental input like string-fragmentation functions and/or cross sections. Both approaches have their merits. While the ones based on effective Lagrangians permit to study certain aspects of QCD (e.g. chiral symmetry) and their manifestation in the space-time evolution of a highly excited strongly interacting system, the phenomenological approaches are very helpful in the interpretation of the data.

The approach presented in this paper is closer in spirit to the transport theories based on effective Lagrangians. We propose a Vlasov equation for the evolution of partons, where the medium dependent mass is directly obtained from QCD, more precisely from the results of lattice calculations. We concentrate on the transport properties of the QGP close to the phase transition, but do not describe hadron dynamics. The lattice calculations for QCD at finite temperature show a phase transition at a critical temperature T_c which separates the regime of the QGP from the one of the hadrons. Two aspects are related to the phase transition: restoration of chiral symmetry and confinement. They manifest themselves in rapid temperature variations around T_c of the chiral

condensate and the Polyakov loop, respectively. Both aspect are contained in the results (often called "data") of lattice calculations.

The basic assumption of our approach is the quasi-particle picture, with an effective mass m , which in thermal equilibrium depends on the temperature T , and on space time (x, t) , in the non-equilibrium situation. We treat the equilibrium case in Sec. II of our paper and show, how $m(T)$ can be obtained from results of the lattice calculations. Sec. III deals with the non-equilibrium case, where $m(x, t)$ is calculated from the same gap-equation as $m(T)$. We report results of a numerical calculation for the expansion of a parton plasma, which shows confinement. The relation to other models is given in Sec. IV.

II. THERMODYNAMICS OF THE DECONFINEMENT PHASE TRANSITION IN A QUASI-PARTICLE APPROACH

The quasi-particle model is one of the most simple approximations to an interacting many body system. A system which consists of particles with definite mass and interactions among them is replaced by a system of non-interacting quasi-particles whose masses $m(T)$ are chosen so that the thermodynamics of the original system is best approximated. For the case of QCD we make an ansatz for the pressure density (thermodynamic potential) for the partons [4]:

$$P_{qp}(m_1, m_2, \dots, T) = \sum_i g_i \int \frac{d^3p}{(2\pi)^3} \frac{p^2}{3E_i(p)} f_i(E_i(p)) - V(m_1, m_2, \dots), \quad (1)$$

where the sum runs over the parton species i with degeneracy factor g_i and where $f_i(E_i(p))$ are Bose or Fermi distribution functions, which depend on the quasi-particle energies $E_i(p) = \sqrt{p^2 + m_i^2}$. $V(m_1, m_2, \dots)$ describes the mean-field contribution to the dispersion relation [4]. The potential density V contributes nontrivially to the thermodynamic relations whenever the masses are temperature dependent.

The masses m_i appearing in the pressure are phenomenological parameters which have to be chosen so that the thermodynamic potential (1) has a minimum,

$$\left(\frac{\partial P}{\partial m_i} \right)_T = 0, \quad i = 1, 2, \dots, \quad (2)$$

leading to :

$$\frac{\partial V}{\partial m_i} + g_i \int \frac{d^3 p}{(2\pi)^3} \frac{m_i}{E_i} f_i(E_i) = 0 . \quad (3)$$

These equations have the form of a gap equation for the masses $m_i(T)$ provided the potential density $V(m_1, m_2, \dots)$ is given. Eq. (3) is equivalent to the consistency relations [4,5] allowing to obtain the energy density from the pressure (1), in the form as for the ideal gas :

$$\begin{aligned} \epsilon_{qp}(T) &= \sum_i g_i \int \frac{d^3 p}{(2\pi)^3} E_i f_i(E_i) + V(T) \\ &= \epsilon_{kin}(m, T) + V(T) , \end{aligned} \quad (4)$$

where $V(T) = V(m_1(T), m_2(T), \dots)$.

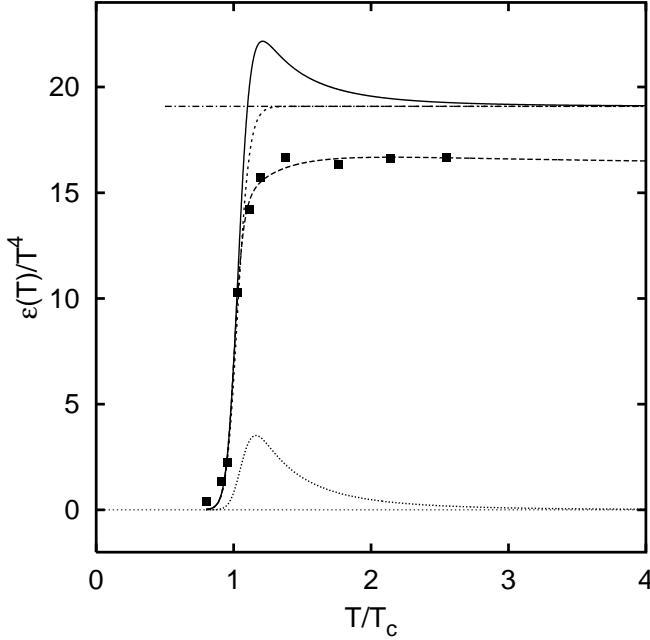


FIG. 1. The energy density of the four-flavor QCD divided by T^4 as a function of the scaled temperature T/T_c . The points are from the lattice data [6]. The solid line is the result of the quasiparticle model described in the text with the chiral symmetry restoration (case (b) and solid line in Fig. 2). The short-dashed and the dotted lines are the corresponding kinetic energy density and potential energy density respectively. The dashed line represents the energy density obtained as a parameterization of the data points and leading to the parton mass increasing at high temperature, (case (a) and dashed line in Fig. 2). The dashed-dotted line indicates the Stefan-Boltzmann limit.

We want to model the deconfinement phase transition of QCD in a quasi-particle approach and therefore have to set a criterion how to determine the quasi-particle

masses $m_i(T)$ or equivalently the mean-field energy density $V(T)$. To date, the most detailed information about the QCD phase transition comes from the lattice calculations which give various thermodynamic functions, among them the energy density $\epsilon_{lat}(T)$. We define our quasi-particle approach by the requirement

$$\epsilon_{qp}(T) = \epsilon_{lat}(T) . \quad (5)$$

Since Eq. (5) is only one relation, only one function $m(T)$ can be determined. We therefore have to assume that our quasi-particle system consists of just one kind of massive partons ($i = 1$ in Eqs. (1) to (4)). We will assume a Boltzmann type distribution function $f(E, T) = \exp^{-\beta E}$. The right hand side in Eq. (5) being given, this equation is a constraint on the unknown function $m(T)$ in $\epsilon_{qp}(T)$. We note that the quasi-particle model constrained by Eq. (5) describes exactly the energy density of lattice QCD, but may reproduce other thermodynamic function only approximately [4,5] which is not a surprise since lattice QCD is not a quasi-particle gas. The functional form for $m(T)$ can be obtained by solving the differential equation

$$\begin{aligned} \frac{dm(T)}{dT} &= \left(\frac{d\epsilon_{lat}(T)}{dT} - \frac{\partial \epsilon_{kin}(m, T)}{\partial T} \right) \\ &\quad / \left(\frac{\partial \epsilon_{kin}(m, T)}{\partial m} + \frac{dV}{dm} \right) , \end{aligned} \quad (6)$$

which is obtained from Eq. (5) by differentiating both sides with respect to T and where dV/dm is given by the gap equation (3). Eq. (6) is a first order differential equation which determines $m(T)$ for a given energy density $\epsilon_{lat}(T)$ and for an initial value $m(T_0)$. Then $V(T)$ can be obtained from $V(T) = \epsilon_{lat}(T) - \epsilon_{kin}(m(T), T)$. The lattice data are normalized so that $\epsilon_{lat}(T) \rightarrow 0$ for $T \rightarrow 0$. It requires that $V(T) \rightarrow 0$ at low temperatures. If $m(T)$ is not obtained from Eq. 6 but is given from some other considerations, the gap equation can be integrated to obtain the potential $V(T)$:

$$V(T) = -g \int_{m(T_0)}^{m(T)} dm \int \frac{d^3 p}{(2\pi)^3} \frac{m}{E(p)} f(E(p)) + V(T_0) , \quad (7)$$

where $g = \sum_i g_i$.

We apply the above methods to the lattice data from [6] shown in Fig. 1. These data are calculated for 4 flavors, corrected for finite lattice size and extrapolated to massless fermions. We use $g = 62.8$ corresponding to the noninteracting limit of QCD with 4 massless flavors. We draw the attention to the fact that the lattice data in Fig. 1 for $\epsilon_{lat}(T)/T^4$ do not approach the Stefan-Boltzmann limit for $T \gg T_c$. This may have two reasons.

- (a) The parton mass $m(T)$ never approaches the chiral limit $m = 0$. Perturbative arguments (whose validity is questionable around T_c) suggest that $m(T) \sim$

T for large T . If we attribute the discrepancy between $\epsilon_{lat}(T)/T^4$ and the Stefan-Boltzmann limit to this reason, one finds the minimal mass $m(T) \simeq 2.1T_c$ right above T_c and $m(T) \simeq 1.1T$ for large T .

- (b) Chiral restoration requires that $m(T) \rightarrow 0$ above the phase transition at least for the fermions. Then the deviation from the Stefan-Boltzmann limit has to be attributed to a mechanism which is outside the scope of the quasi-particle approach.

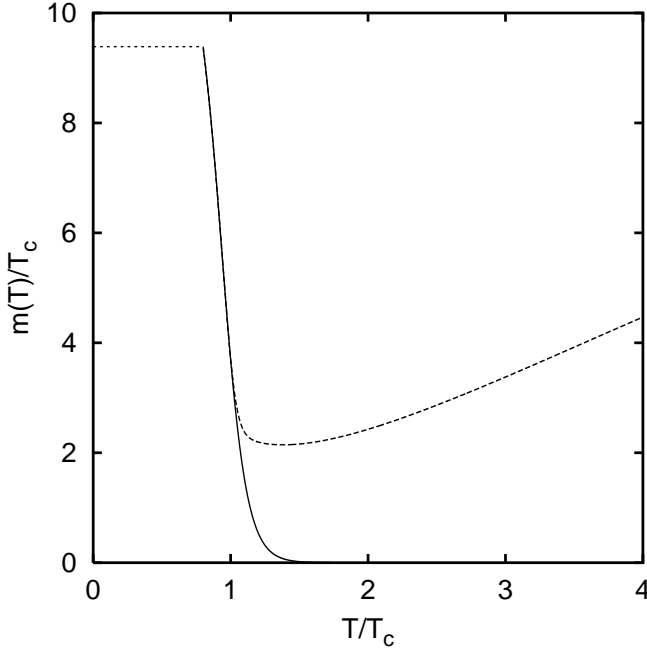


FIG. 2. The dashed line represents the temperature dependence of the quasiparticle mass as obtained from the lattice data (case (a)). The short dashed line represents the extrapolation to the low temperature region. It is taken to be constant, and suffices to effectively confine the partons (an absolute confinement would require that the mass goes to infinity at low temperatures). The solid line represents the assumed temperature dependence of the parton mass with zero limit at high temperature (case (b)).

We will explore both possibilities and call the corresponding masses $m_a(T)$ and $m_b(T)$ respectively. First we solve the Eq. (6) to obtain $m_a(T)$ for the case (a), where we set $m_a(T_0) = 9.5T_c$ for $T_0 = 0.8T_c$. For the case (b) we take $m_a(T)$ obtained in (a) for $T < T_c$ and extrapolate it at $T > T_c$ so that $m(T) \rightarrow 0$ at large T (Fig. 2). From this new functional form $m_b(T)$ we obtain $V_b(T)$ and $\epsilon_b(T)$ via Eq. (7). Fig. 2 shows the obtained temperature dependence of the parton mass for the two cases. While the two functions $m(T)$ coincide in the region of the confinement transition (below T_c) they differ dramatically for

$T > T_c$. The mass $m_a(T)$ increases linearly with T for large temperatures while $m_b(T)$ is set to reach the chiral limit at high temperatures. Fig. 1 also shows also the energy density corresponding to the two cases. We observe that in the case (a) $\epsilon_{qp}(T)$ follows the lattice points as it should. In particular it has the same high temperature limit which is different from the Stefan-Boltzmann limit.

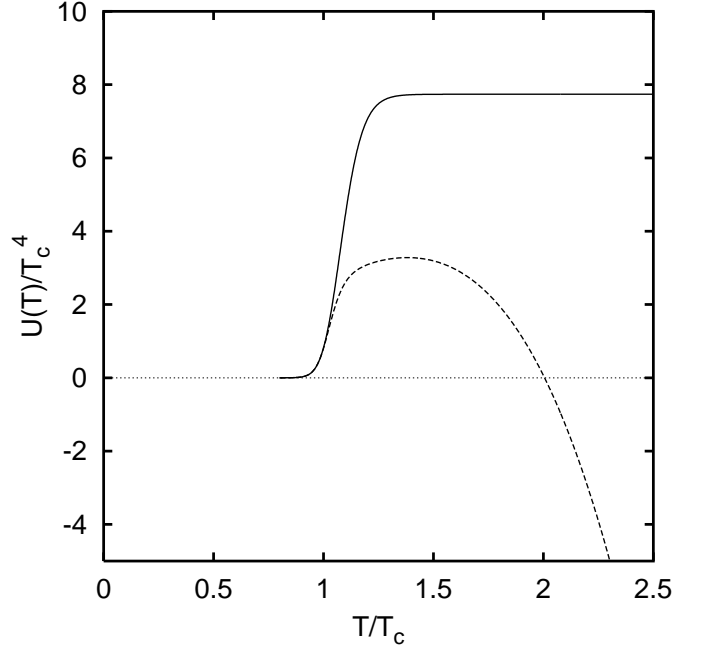


FIG. 3. The potential energy density $V(T)$ as a function of the temperature for the case (a) and (b) of the temperature dependence of the mass, dashed and solid line respectively.

The energy density for the case (b) is different for $T > T_c$ and approaches the Stefan-Boltzmann limit. Fig. 1 also shows the densities for the kinetic energy $\epsilon_{kin}(m(T), T)$ and for the potential energy $V(T)$ for the case (b). Fig. 3 shows the potential density functions $V(T)$ for both cases. In the case (b), one can identify the large temperature limit of $V_b(T)$ with the bag constant B , since $V_b(T = 0) = 0$. Indeed for large T (in the deconfined phase) Eqs. (1) and (4) take the form of the free massless gas with a bag constant $B = V_b(T = \infty)$. For the case (a) one can *define* the bag constant as the value of the potential density $V_a(T)$ for the temperature where the mass $m_a(T)$ is the smallest (slightly above T_c). We find

$$B^{1/4} = \begin{cases} 1.35T_c = 240 \text{ MeV} & \text{for case (a)} \\ 1.67T_c = 300 \text{ MeV} & \text{for case (b)} \end{cases} \quad (8)$$

for a value of $T_c = 180 \text{ MeV}$ corresponding to four-flavor QCD. The order of magnitude of the bag constant is cor-

rect, but in order to compare it to the usual bag constant ($B^{1/4} = 135 - 200$ MeV) one should use the lattice results for the energy density and the critical temperature of the two-flavor QCD as an input for the quasi-particle parton model.

In order to distinguish between the two solutions for $m(T)$ we investigate the temperature dependence of the chiral condensate in the quasi-particle picture

$$\langle \bar{\Psi}\Psi \rangle_{qp}(T) = \langle \bar{\Psi}\Psi \rangle_{vac}(T) + g_{q\bar{q}} \int \frac{d^3p}{(2\pi)^3} \frac{m}{E} f(E), \quad (9)$$

where $g_{q\bar{q}}$ counts fermion and anti-fermion degrees of freedom and the vacuum part of the chiral condensate is given by an expression including a cutoff in momentum

$$\langle \bar{\Psi}\Psi \rangle_{vac}(T) = g_{q\bar{q}} \int_{|p| < \Lambda} \frac{d^3p}{2(2\pi)^3} \frac{m}{E}. \quad (10)$$

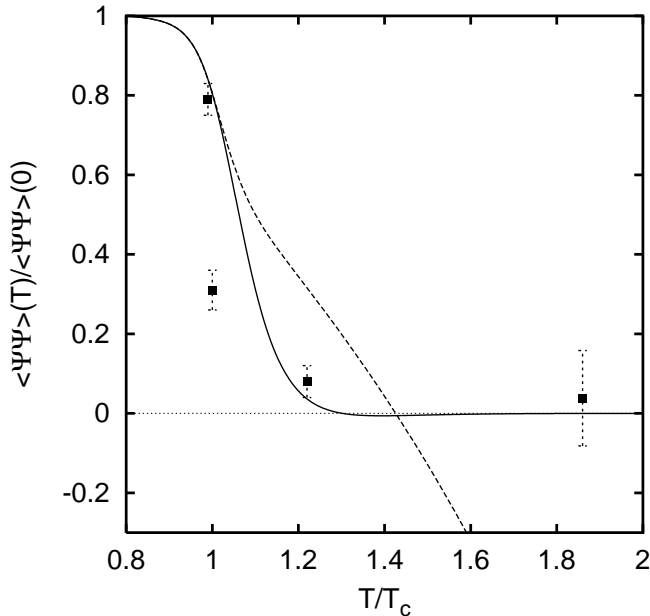


FIG. 4. The chiral condensate as a function of the temperature for the case (a) and (b) of the temperature dependence of the mass, dashed and solid line respectively. The data points are for the lattice data in the four-flavor QCD [7].

The value of the cutoff $\Lambda = 430$ MeV is fixed to reproduce the zero temperature value of the chiral condensate which we take twice the usual value

$$\langle \bar{\Psi}\Psi \rangle_{vac}(0) = 2(250\text{MeV})^4, \quad (11)$$

because we are modeling the four-flavor lattice QCD. Fig. 4 shows a comparison between the condensate functions for the quasi-particle picture and the lattice data.

This comparison clearly favors case (b), where $m(T) \rightarrow 0$ above T_c . In what follows, we will mainly work with this solution.

Before we treat the nonequilibrium case we apply the gap equation to the case of finite density and calculate the density dependence of the parton mass. We introduce variables which will be also useful for the discussion of the nonequilibrium case. First let us write the gap equation in the form

$$\frac{dV}{dm} = V'(\rho) \frac{d\rho}{dm} = -\rho, \quad (12)$$

where we define the scalar density

$$\rho = g \int \frac{d^3p}{(2\pi)^3} \frac{m}{E(p)} f(E(p)). \quad (13)$$

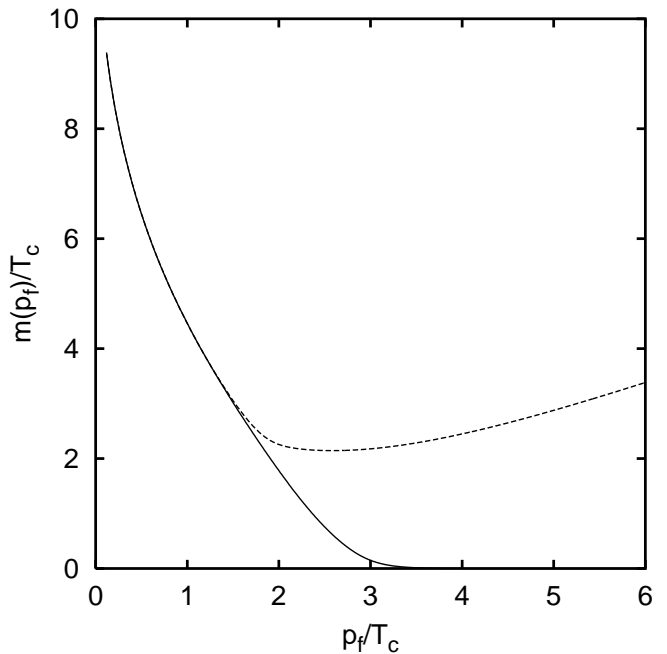


FIG. 5. The quasiparticle mass as a function of the scaled Fermi momentum p_f/T_c . The solid and dashed lines correspond to two different temperature dependences of the parton mass in Fig. 2.

It allows us to use the functions $V(\rho)$ and $m(\rho)$ instead of $V(T)$ and $m(T)$ for the parameterization of the potential energy density and the mass respectively. Assuming that the energy density depends on temperature T and chemical potential μ only through $\rho(T, \mu)$ we can generalize the finite temperature case also to finite density. In principle the potential $V(\rho)$ could depend on other quantities, e.g. the baryon density. Any such more general case cannot

be discussed using only the lattice data at finite temperature. As a support for our assumption we note that for the NJL model the potential density V depends only on the density ρ (Sec. IV).

We write the gap equation (3) at finite density

$$\frac{dV}{dm} = -g_f \int \frac{d^3p}{(2\pi)^3} \frac{m}{E(p)} \Theta(p_f - |p|), \quad (14)$$

where g_f counts the number of fermion degrees of freedom. Note that here we are using the Fermi distribution for the fermions at finite density and zero temperature and $V(m)$ from the lattice data. Fig. 5 shows the mass of the partons as a function of the Fermi momentum p_f . The behavior is similar as in the finite temperature case. For low density the mass increases leading to the effective confinement. At high density the mass is proportional to p_f for the case (a) and goes to zero in the case (b).

III. TRANSPORT THEORY OF THE EFFECTIVE CONFINING MODEL

In this section we will discuss the nonequilibrium evolution of the parton densities. In the semiclassical limit the collisionless plasma of quasi-particle partons can be described by the Vlasov equation for the phase-space distribution function $f(x, t, p)$:

$$\partial_t f(x, t, p) + \frac{p}{E(p, x, t)} \nabla_x f(x, t, p) - \frac{m(x, t)}{E(p, x, t)} \nabla_x m(x, t) \nabla_p f(x, t, p) = 0. \quad (15)$$

Eq. (15) has to be supplemented by an equation for the space-time dependent mass $m(x, t)$. A sufficient condition for the requirement, that the Vlasov equation describes the same physics at thermal equilibrium as presented in the previous section is that $m(x, t)$ satisfies the same gap equation

$$\frac{dV}{dm} = -g \int \frac{d^3p}{(2\pi)^3} \frac{m(x, t)}{E(p, x, t)} f(x, t, p) = -\rho(x, t), \quad (16)$$

where the thermal distribution function $f(E)$ in Eq. (3) has been replaced by the nonequilibrium solution of the Vlasov equation $f(x, t, p)$ and where $V(m)$ is the same as in equilibrium. The solution of the nonequilibrium gap equation is then a function $m(x, t)$ of space and time. Eq. (16) is however not the most general equation which reduces to the equilibrium finite temperature gap Eq. (3), but one can add to it terms which depend on the spatial and time derivatives of $m(x, t)$. We will come back to this question in Sec. IV. Here we note that the choice in Eq. (16) guarantees that the total energy of the system

$$E(t) = g \int d^3x \int \frac{d^3p}{(2\pi)^3} E(p, x, t) f(x, t, p) + \int d^3x V(\rho(x, t)) \quad (17)$$

is conserved by the evolution according to the Vlasov Eq. (15), i.e. the energy of the system is constant.

We have numerically solved the Vlasov equation together with the gap equation for the two cases of the functional dependence of the mass $m(T)$ on the temperature discussed in Sec. II, but most of the results shown relate to the case where the chiral condensate vanishes at high temperatures (case (b) in the previous section). We have used the test particle method for the solution of the Vlasov equation, i.e. we have made the ansatz

$$f(x, t, p) = \sum_{j=1}^N \delta^3(x - x_j(t)) \delta^3(p - p_j(t)), \quad (18)$$

where the trajectories $x_j(t)$ and $p_j(t)$ of the N test particles satisfy Hamilton's equations with

$$H(x, p) = \sqrt{p^2 + m^2(x, t)}. \quad (19)$$

The initial conditions $x_j(0)$ and $p_j(0)$ are chosen so that given initial densities for matter and momentum are reproduced. The initial density is chosen spherically symmetric. Also in the solution of the gap equation the spherical symmetry is imposed by angle averaging.

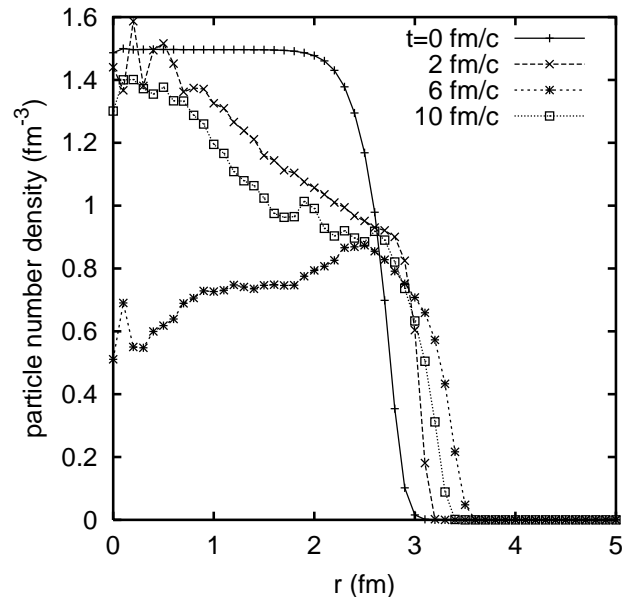


FIG. 6. The parton density distribution at different times, as obtained from the nonequilibrium evolution of the initial fireball ($t = 0$).

At time $t = 0$ the system is described by the density profile shown in Fig. 6 and with a momentum distribution corresponding to a temperature $T = 1.3T_c = 180$ MeV. Fig. 6 shows the density for different times. The system expands for $t = 2$ and 6 fm/c, but then comes

back ($t = 10$ fm/c). The dependence of $m(x, t)$ on the radius at different times is shown in Fig. 7. As expected

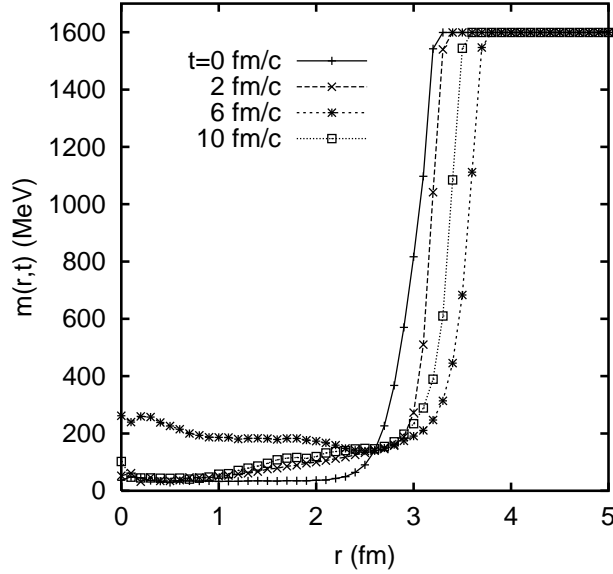


FIG. 7. The parton mass distribution at different times, as obtained from the nonequilibrium evolution of the fireball.

the mass is small in the interior and increases towards the surface. This increase is responsible for the confinement. Indeed one can show that the equation of motion of one particle in the mean-field of the other particles conserves the energy of the particle $\sqrt{p^2 + m^2}$. Thus a particle cannot leave the region of deconfined plasma, if its initial momentum p satisfies:

$$p^2 < m_{vac}^2 - m^2, \quad (20)$$

where m_{vac} is the parton mass in vacuum and m is the initial selfconsistent mass of the parton inside the plasma. The vacuum mass should be infinite, if the confinement is absolute. In our calculation we take the vacuum mass equal to $\sim 9.4T_c$ (see Fig. 2), which effectively confines the partons at the temperatures discussed here. Thus the partons cannot leave the hot fireball if their initial momentum is smaller than $\sim 9.4T_c$, which is the case for most of the partons at our initial temperature.

Figs. 8 and 9 show the time development of the momentum p_x and the coordinate x of a particular test particle. The particle oscillates between the borders of the fireball and at the border its momentum is reduced and eventually reversed by the action of the force:

$$\frac{dp}{dt} = -\frac{m}{E} \nabla_x m. \quad (21)$$

In contrast to the simple particle motion, partons traveling in bunches may leave into the vacuum region, since

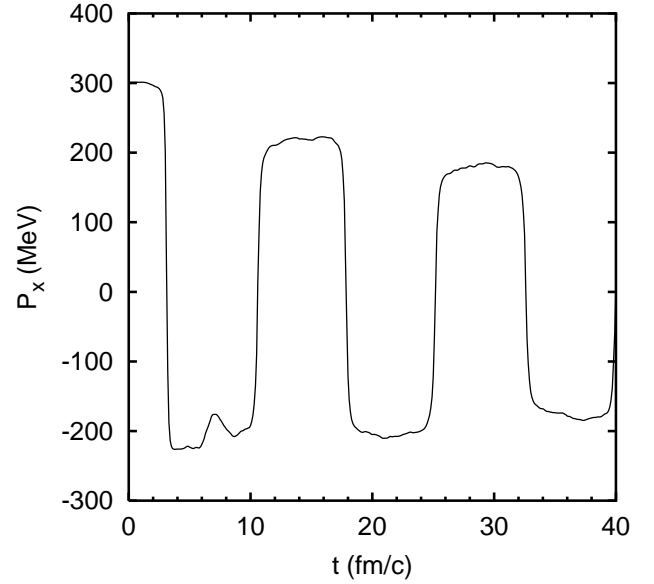


FIG. 8. The component p_x of the momentum of a particular test-particle taken from the simulation of the time evolution of the region of deconfined plasma.

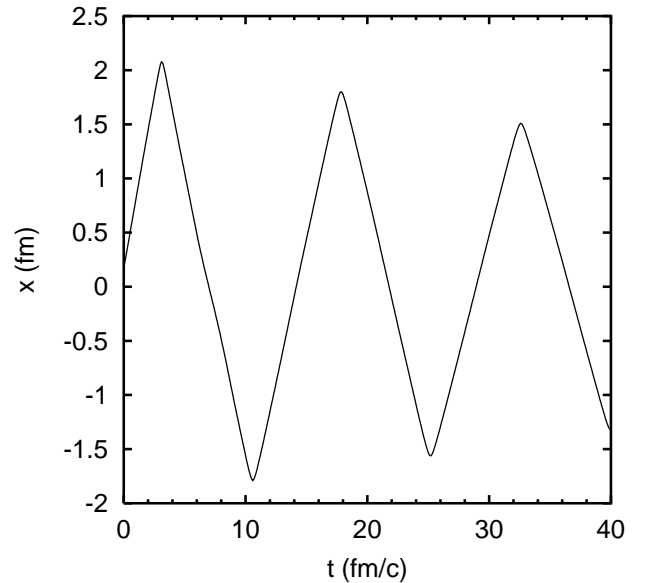


FIG. 9. The x coordinate of the same test-particle as in Fig. 8.

the internally created field leads to small masses inside the bunch. This possibility is excluded in our method of

solution, since we require at each time step that the system stays spherically symmetric. This mechanism then generates collective vibrations of the surface of the fireball, when particles are trying to leave the hot region

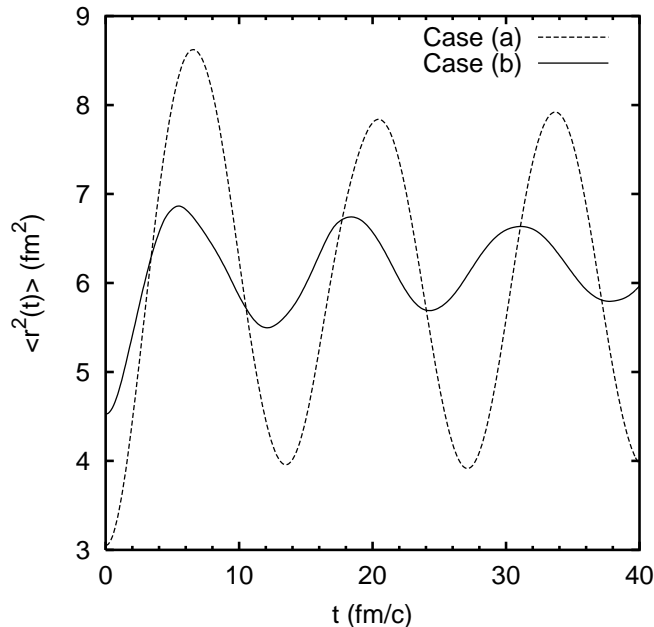


FIG. 10. The time evolution of the mean square radius of the region of deconfined plasma for the case (a) and (b), dashed and solid line respectively

simultaneously. Fig. 10 shows the time dependence for the mean square radius of the fireball :

$$\langle r^2(t) \rangle = g \int d^3x \, x^2 \int \frac{d^3p}{(2\pi)^3} f(x, t, p) . \quad (22)$$

The oscillation which can be seen on the figure reflect the collective monopole oscillations of the parton density, with partons leaving the fireball and reflected back when their mass grows. Analogous collective oscillations have been observed in the Vlasov evolution of the nucleon in the Friedberg-Lee model [8].

As the volume of the fireball oscillates, its potential energy will also oscillate growing for large volumes and decreasing when the system is compressed. The period of the collective oscillations is basically determined by the time which a particle needs to travel from one border of the fireball to the other (Fig. 9). For massless deconfined partons (case (b) in Sec. II) this time is twice the radius of the system divided by the speed of light. The total energy is of course conserved (see Fig. 11), to the accuracy of our numerical solution, and the kinetic (and then also the potential energy) has oscillations of the same period as the oscillations of the mean square radius in Fig. 10.

We mention the possibility of fragmentation of the fireball into smaller pieces, each of them having large par-

ton density inside and thus a small mass of partons. This fragmentation mechanism cannot be studied in our spherically symmetric mean-field theory. It would require a description including the fluctuations of the density.

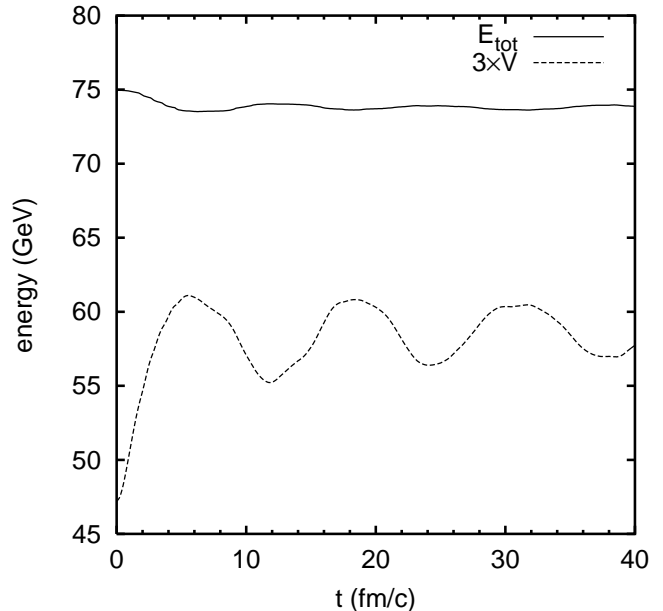


FIG. 11. The time dependence of the total and potential energy of the parton plasma, solid and dashed lines respectively

We state the main result of this section: the Vlasov equation together with the gap equation based on lattice data shows confinement. For not too high initial temperatures the fireball stays compact. Of course the surface of the fireball can oscillate, but the system remains bounded. This behavior is in contrast to the free expansion of the parton gas, where the parton fireball would start to expand and cool down faster. In our picture the partons are confined, since no hadronization is included (see Fig. 10).

IV. RELATION TO OTHER EFFECTIVE MODELS

The effective models of the QCD using parton degrees of freedom are mostly restricted to the fermion sector. Thus NJL type models [2] have only fermionic degrees of freedom with four-fermion interaction. At high temperature and/or density the quarks are massless or almost and at low densities due to the nonzero quark-condensate they acquire a finite mass with value around 350 MeV. The quarks are not confined in this theory. The NJL gap equation for the quark mass can also be written in the form of Eq. (3) where dV/dm is defined by the expression

$$\frac{dV}{dm} \equiv \frac{(m - m_0)}{2G} - 6N_f \int_{|p| < \Lambda} \frac{d^3p}{(2\pi)^3} \frac{m}{E}, \quad (23)$$

where G is the four fermion coupling constant, Λ is the infrared cutoff, m_0 is the current quark mass and N_f is the number of flavors. Fig. 12 shows a comparison between the potential extracted from lattice calculations and the one from the NJL model. The difference is twofold: (i) Shape: While the potentials for Friedberg-Lee and NJL model show a clear minimum at the position of the constituent mass in the vacuum, the potential from our approach drops monotonically to zero, reflecting the confinement (infinite vacuum mass). (ii) Magnitude: At $m = 0$ the potential from our approach differs by about a factor 5 from the other approaches. This may be partly due to the different numbers of degrees of freedom. While Friedberg-Lee and NJL refer to a two-flavor quark theory (no gluons), the lattice calculation is performed for $N_f = 4$ and gluons. The remaining difference may be due to quantitative difference between the four-flavor and the two-flavor QCD, which goes beyond a simple rescaling of the number of degrees of freedom.

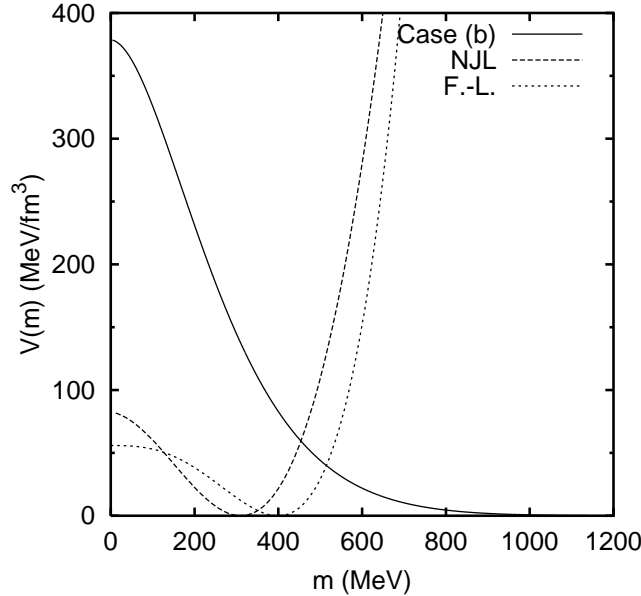


FIG. 12. The potential energy density $V(m)$ as a function of the mass as extracted from lattice QCD (solid line), for the two-flavor NJL model (dashed line) and for the Friedberg-Lee model (dotted line). We used $T_c = 140$ MeV in defining $V(m)$. The large value of the bag constant $B = V(m = 0)$ for the potential density from the lattice data can be due to a larger number of degrees of freedom in the four-flavor model.

The Friedberg-Lee model describes fermions coupled to a scalar field $\sigma(x, t)$ which plays the role of an effective mass and whose dynamics is driven by a potential $U(\sigma)$.

Of course as in the NJL model the degrees of freedom are restricted to the fermions. The Lagrangian of the Friedberg-Lee model can be written as:

$$\mathcal{L} = \bar{\Psi}(i\gamma^\mu \partial_\mu)\Psi - g\sigma\bar{\Psi}\Psi + \frac{1}{2}\partial_\mu\sigma\partial^\mu\sigma - U(\sigma), \quad (24)$$

where the fermion field operator Ψ also carries the flavor and color indices. The effective quark mass $g\sigma$ can include also a contribution from the current quark mass.

When the expectation value of the σ field is infinity, the quarks are confined. The same is also effectively true if the vacuum expectation value of the σ field is very large. The gap equation for the quark mass σ is given by the classical equation of motion for the σ field:

$$\square\sigma + U'(\sigma) = -g\langle\bar{\Psi}\Psi\rangle(x, t). \quad (25)$$

In the case of homogeneous systems $\square\sigma = 0$ (e.g. in the mean-field thermodynamics) the Friedberg-Lee gap equation is equivalent to the gap equation used in Sec. II if $V(m) = U(\sigma)$. In particular the thermodynamical energy density discussed in Sec. II can be reproduced in the Friedberg-Lee model if not for the neglect of the gluon degrees of freedom. The difference between our approach and the one by Friedberg and Lee rests in the choice of the potential. While they assume certain forms, we let $V(m)$ be determined by the lattice data. One should note that in the homogeneous systems the confining Friedberg-Lee model, with the fermion mass $m = \kappa(\sigma)$ being a function of the field σ , is also equivalent to our approach after a change of variables $\sigma \rightarrow m$. The infinite value of the fermion mass means simply in the language of Eq. (24), that the vacuum gap equation $dV/dm = 0$ has a solution at $m = \infty$.

The kinetic term for the σ makes a difference for the case of nonequilibrium or nonhomogeneous systems. In the dynamical evolution of a nonequilibrium system in the Friedberg-Lee model, the σ field is another dynamical field not related to the local value of the scalar density ρ [8]. The inclusion of the kinetic term for the σ field however leads to the problem that the value of the σ field can go negative. The potential $U(\sigma)$ cannot be extracted for the negative values of σ from the lattice data. Moreover in the cases when the mass of the fermion field becomes negative, its evolution cannot be described by a semiclassical Vlasov equation.

V. DISCUSSION

The description of the deconfinement transition in heavy ion collisions is a very important theoretical problem. A realistic description could allow to define which observables are relevant for the observation of the quark-gluon plasma formation. A dynamical simulation is wished for in order to extract the properties of the plasma from the experimental data. Any such approach meets difficulties in the description of the confinement and of

the hadronization transition when the temperature of the deconfined region drops down. In the present work we have addressed only a part of this program, namely the influence of the confinement on the dynamics of partons.

The confinement of partons below T_c is described in a quasi-particle gas model by the increase of the parton mass at low energy densities. The temperature dependence of the parton mass is extracted from the lattice data. In the range of temperatures analyzed ($0.8T_c < T < T_c$) the mass of the partons increases to values which effectively confine the quarks and gluons. The requirement of the restoration of the chiral symmetry at high temperatures fixes the temperature mass dependence for $T > T_c$.

The formalism is generalized to the nonequilibrium case. The time development of a deconfined fireball studied in a Vlasov equation is different from what is usually discussed in the literature, in that it shows confinement. The expansion of the system is forbidden, but instead we observe collective oscillations of the parton plasma. The time scale of these oscillations in the collisionless plasma is determined by the size of the deconfined region. This time scale should be compared to the hadronization time in order to determine if the oscillation could develop.

The increase of the parton mass has implication also for the hydrodynamical model of the plasma expansion. The slowing down of the hydrodynamic expansion is observed in simulations of systems with first order phase transition [9] or in a hydrodynamical calculation with the NJL model [10]. The use of a confining mass in the hydrodynamical model would stop the expansion. Further expansion of the fireball is possible only after hadronization.

If the hadronization takes place mainly at the surface of the deconfined phase then the dynamics of the system could be described by a hydrodynamical model with first order phase transition. However, the description using the transport equation allows to discuss alternative scenarios of the hadronization, e.g. hadronization due to parton collisions in the plasma [11] with possible softening of the spectra of produced mesons. Another hadronization mechanism could be the fragmentation of the fireball due to a possible instability of the system at finite baryon density [12] or due to dynamical instabilities present for energy densities corresponding to a mixed phase in the case of a first order phase transition. The discussion of the hadronization mechanism and the inclusion of the dynamics of mesons remains to be done.

ACKNOWLEDGMENTS

One of the authors (P.B.) wishes to thank the Alexander von Humboldt Foundation for financial support. This work has been supported in part by the German Ministry for Education and Research (BMBF) under contract number 06 HD 742.

* on leave from: Institute of Nuclear Physics, Cracow, Poland

- [1] R. Friedberg and T.D. Lee, Phys. Rev. D **15**, 1694 (1977); Phys. Rev. D **16**, 1096 (1977). L. Wilets, Nontopological Solitons, (World Scientific, Singapore, 1989).
- [2] Y. Nambu and G. Jona-Lasinio, Phys. Rev. **122**, 345 (1961); **124**, 246 (1961). U. Vogl and W. Weise, Prog. Part. Nucl. Phys. **27**, 195 (1991); S.P. Klevansky Rev. Mod. Phys. **64**, 649 (1992); T. Hatsuda and T. Kunihiro, Phys. Rep. **247**, 221 (1994).
- [3] K. Werner, Phys. Rep. **232**, 87 (1993); H. Sorge, Phys. Rev. C **52**, 3291 (1995); Y. Pang, T.J. Schlagel and S.H. Kahana, Nucl. Phys. **A544**, 435 (1992); K. Geiger, Phys. Rep. **258**, 237 (1995); X.-N. Wang and M. Gyulassy, Phys. Rev. D **44**, 3501 (1991).
- [4] M.I. Gorenstein and S.N. Yang, Phys. Rev. D **52**, 5206 (1995).
- [5] A. Peshier, B. Kämpfer, O.P. Pavlenko and G. Soff, Phys. Rev. D **54**, 2399 (1996); P. Lévai and U. Heinz, hep-ph/9710463.
- [6] J. Engels et al. , Phys. Lett. B **396**, 210 (1997).
- [7] F. Karsch, Nucl. Phys. **A590**, 367 (1995).
- [8] S. Loh, C. Greiner, U. Mosel and M.H. Thoma, Nucl. Phys. **A619**, 321 (1997).
- [9] D.H. Rischke, Nucl. Phys. **A610**, 88 (1996); C.M. Hung and E.V. Shuryak, hep-ph/9709264.
- [10] I.N. Mishustin, J.A. Pedersen and O. Scavenius, hep-ph/9801314.
- [11] J. Dolejsi, W. Florkowski and J. Hüfner, Phys. Lett. B **349**, (1995) 18.
- [12] R. Rapp, T. Schäfer, E.V. Shuryak and M. Velkovsky, hep-ph/9711396; M. Alford, K. Rajagopal and F. Wilczek, hep-ph/9711395.